

# Identifying Unique Protein Alterations Caused by SPTLC1 Mutations in a Transfected Neuronal Cell Model

Scott E. Stimpson<sup>1,2,3\*</sup>, Anu Shanu<sup>1,2,4\*</sup>, Jens R. Coorssen<sup>2,3,4,5#</sup>, Simon J. Myers<sup>1,2,3,4#</sup>

<sup>1</sup>Neuro-Cell Biology Laboratory, Western Sydney University, Penrith, Australia

<sup>2</sup>Molecular Medicine Research Group, Western Sydney University, Penrith, Australia

<sup>3</sup>School of Science and Health, Western Sydney University, Penrith, Australia

<sup>4</sup>School of Medicine, Western Sydney University, Penrith, Australia

<sup>5</sup>Molecular Physiology, Western Sydney University, Penrith, Australia

Email: #s.myers@uws.edu.au, #jcoorssen@brocku.ca

**How to cite this paper:** Stimpson, S.E., Shanu, A., Coorssen, J.R. and Myers, S.J. (2016) Identifying Unique Protein Alterations Caused by SPTLC1 Mutations in a Transfected Neuronal Cell Model. *World Journal of Neuroscience*, 6, 325-347.  
<http://dx.doi.org/10.4236/wjns.2016.64035>

**Received:** August 17, 2016

**Accepted:** November 27, 2016

**Published:** November 30, 2016

Copyright © 2016 by authors and Scientific Research Publishing Inc. This work is licensed under the Creative Commons Attribution International License (CC BY 4.0).

<http://creativecommons.org/licenses/by/4.0/>



Open Access

## Abstract

Hereditary sensory neuropathy type I is an autosomal dominant disorder that affects the sensory neurons. Three missense mutations in serine palmitoyltransferase long chain subunit 1 cause hereditary sensory neuropathy type I. The endoplasmic reticulum, where the serine palmitoyltransferase long chain subunit 1 protein resides, and mitochondria are both altered in hereditary sensory neuropathy type I mutant cells. Employing a transfected neuronal cell line (ND15), we have identified and confirmed altered protein expression levels of ubiquinol cytochrome C, Hypoxia Up regulated Protein 1, Chloride Intracellular Channel Protein 1, Ubiquitin-40s Ribosomal Protein S27a, and Coactosin. Additionally, further 14 new proteins that exhibited altered expression within V144D, C133W and C133Y mutants were identified. These data have shown that mutations in SPTLC1 alter the expression of a set of proteins that may help to establish a causal link between the mitochondria and ER and the “dying back” process of dorsal root ganglion neurons that occurs in HSN-I.

## Keywords

Hereditary Sensory Neuropathy Type 1, ND15, SPTLC1, ER Stress, Coactosin

## 1. Introduction

Hereditary Sensory Neuropathy type I (HSN-I) is an autosomal dominant inherited neurodegenerative disorder. It is caused by missense mutations in the open reading

\*Both authors contributed equally

frame of serine palmitoyltransferase (SPT) long chain subunit 1 (SPTLC1) [1], causing amino acid substitutions from cysteine to tryptophan at position 133 (C133W), cysteine to tyrosine at position 133 (C133Y) or valine to aspartate at position 144 (V144D) [1]. SPT is an Endoplasmic Reticulum (ER) bound and a key rate-determining enzyme in the complex sphingolipid metabolic pathway [2]. HSN-I is characterised by degeneration in the Dorsal Root Ganglion (DRG) and presents with clinical onset between the second or third decades of life [2] [3] [4] [5].

In previous studies, we investigated altered protein profile changes in the mitochondria and ER of HSN-I patient cells (SPTLC1 V144D mutation) [6] [7] [8]. Changes in protein expression were identified in both the isolated mitochondria and ER subcellular fractions. Ubiquinol cytochrome C was most notably altered in expression within the mitochondria of the HSN-I patient cells. Within the ER fractions, Hypoxia up regulated Protein 1 (ORP-150), Chloride Intracellular Channel Protein 1 (CLIC1), Ubiquitin-40s Ribosomal Protein S27a (RPS27a), and Coactosin (COTL1) protein expression were increased in the HSN-I patient cells (SPTLC1 V144D mutation). In addition to these findings, further 36 proteins were identified from both the mitochondria and ER of HSN-I patients' cells by using top-down proteomic analyses [6] [7] [8]. Of these 36 proteins, the observed alterations were in proteins related to oxidative stress and cytoskeleton.

Based on these earlier findings, this investigation employed ND15 cell line (hybrid of rat dorsal root ganglion neuron and a mouse neuroblastoma) which had been transiently transfected (TT) to overexpress the three SPTLC1 missense mutations: V144D, C133W and C133Y. The data obtained from this ND15 neuronal cell model confirmed previous results from the HSN-I patient lymphoblast, while notably identifying changes exhibited in the C133W and C133Y mutations. We have also identified an additional 14 proteins that are altered in abundance within the transfected ND15 cells. Together these findings offer a greater insight into the molecular mechanisms occurring in the three known mutations causing HSN-I.

## 2. Materials and Methods

### 2.1. ND15 Cell Culture

All cell culture stock solutions, including DMEM, Foetal Bovine Serum (FBS), Penicillin (100 U/mL), Streptomycin (100 µg/mL), L-glutamine (2 M), NEAA (1 M), and phosphate buffered saline (PBS) were purchased from GIBCO Invitrogen (Australia). Cell culture consumables were purchased from BD Falcon (Greiner, USA). ORP-150, CLIC1, RPS27a, Calnexin, ubiquinol cytochrome C, MTCO2, and GAPDH primary antibodies were purchased from Abcam (USA); SPTLC1 primary antibody was purchased from Santa Cruz Biotechnology (USA). COTL1 primary antibody was purchased from Protein SciTech (USA). Kif2A and GFP primary antibodies were purchased from Merck Millipore (USA). Secondary horse radish peroxidase (HRP) mouse antibodies and DAPI stains were purchased from Sigma-Aldrich (Australia). ND15 cell lines were cultured in DMEM media, supplemented with FBS (10% v/v), Penicillin (1 U/mL),

Streptomycin (1 µg/mL), L-glutamine (2 mM), and NEAA (1 mM) at 37°C in a humidified atmosphere of 5% CO<sub>2</sub>, in T75 cm<sup>2</sup> culture flasks (Greiner, Interpath). Prior to use in biochemical assays, ND15s were collected by centrifugation at 1500 ×g (5 min at RT) and washed in PBS. Cell counts were obtained using the Countess Automated Cell Counter (Invitrogen, Australia).

## 2.2. Transient Transfections

ND15 cells were transiently transfected (TT) with plasmid constructs (GFP-tagged SPTLC Wild type, V144D, C133W and C133Y mutants) using Lipofectamine 2000 (L2K; Invitrogen, USA). Cells were plated at a density of  $2 \times 10^5$  per well in 6 well plates. Transfections were carried out when cells were 90% - 95% confluent (approximately 24 hours after plating, at 37°C and 5% CO<sub>2</sub>), according to manufacturer instructions. Briefly, plasmid constructs and L2K reagent were diluted in 250 µL of Opti-MEM I Reduced Serum Media (Invitrogen, USA), to yield 16 µg/ml DNA and 40 µL/ml L2K. Within 5 min of each dilution, the DNA construct diluents and L2K diluents were combined and incubated for 30 min at 25°C. After incubation, DNA-L2K complexes (500 µL) were added into each well, as required. The cells were then incubated at 37°C in a humidified atmosphere of 5% CO<sub>2</sub> for 6 h. Cells then had media replaced with fresh media and were left to incubate for 48 h. Post transfection, cells were harvested and cell lysate was used for further analyses.

## 2.3. Detection of Total Protein Concentration

Determination of total cellular protein was carried out using the EZQ Protein Estimation Assay (Invitrogen, Australia) as previously described [9].

## 2.4. SDS-PAGE and Immunoblotting

Nontransfected, wild type and mutant protein fractions (25 µg total protein) were subjected to SDS-PAGE on 12.5% resolving gels and transferred to PVDF membrane. The membranes were blocked with 5% skim milk in TBS buffer containing 0.1% Tween-20. Whole membranes were blocked and incubated with anti-SPTLC1, anti-GAPDH, anti-ORP-150, anti-CLIC1, anti-RPS27a, anti-COTL1, anti-MTCO2, anti-GFP and anti-Kif2A antibodies respectively, at 1:1000 dilution, for 16 h. Membranes were washed and incubated with secondary HRP antibody (1:2000 dilution) for 1 h at RT. Blots were washed and developed using an enhanced chemiluminescence (ECL) detection kit (Pierce Thermo Scientific, USA). Membranes were developed on CL-Xposure Film (Thermo Fisher Scientific, USA) using an AGFA X-ray developer.

## 2.5. Immunofluorescence

Immunofluorescence was carried out as previously described [6]. Briefly, ND15 cells ( $1 \times 10^6$  cells) were grown on glass coverslips in 6-well plates 24 h prior to transfection. 48 h post transfection, cells were washed and 4% paraformaldehyde was added for 15 min. Following incubation, cells were washed and placed in 0.5% TritonX-100 and incubated

at 37°C for 20 min. The cells were then blocked in 5% BSA solution at 37°C for 30 min, then incubated in primary antibody against SPTLC1, Kif2A, Cytochrome C, RPS27a, CLIC1, ORP-150, COTL1, Calnexin and MTCO2, and incubated for 1 h at RT. The cells were subsequently washed and incubated in secondary antibody, anti-mouse Rhodamine (Millipore, 1:200), for 1 h at RT. Nuclei were stained with DAPI (1 µg/µL) for 2 min, after which the cells were washed and dried overnight. The coverslips were then mounted onto glass slides prior to confocal imaging using the LSM 5 confocal microscope comprising the LSM 5 exciter laser scanning microscope with Axiovert 200 M inverted optical microscope (Carl Zeiss, Jena, Germany).

## 2.6. Flow Cytometry

FACS analyses were carried out as previously described [6]. ND15 cells were transfected as above, and cells were then suspended in 4% paraformaldehyde and incubated for 15 min at RT and then resuspended in 0.3% Triton X-100 for 15 min at 37°C. After incubation the cell suspension was centrifuged at 1000 ×g for 5 min and the pellet resuspended in primary antibody for 1 h at RT. Cell suspension was centrifuged, washed in PBS and resuspended in secondary antibody, anti-mouse or anti-rabbit Rhodamine (Millipore, 1:200) for 1 h at RT. The cell suspension was then analysed using the MACSQuant flow cytometer (Miltenyi Biotech, Germany).

## 2.7. Two Dimensional Gel Electrophoresis

2DE was carried out as previously described [6] [10] [11] [12] using a total of 100 µg protein for each analysis. Briefly, whole ND15 proteins were reduced and alkylated in solutions containing total protein extraction buffer (containing 8 M urea, 2 M thiourea and 4% CHAPS without ampholytes), total extraction buffer with 2% ampholytes, TBP/DTT disulphide reduction buffer (2.3 mM Tributyl phosphine and 45 mM DTT) and alkylation buffer (230 mM acrylamide monomer).

The treated samples were added to 7 cm Non-Linear pH 3 - 10 IPG strips (Bio-Rad ReadyStrip), and rehydrated for 16 h at RT. Isoelectric focusing (IEF) was then carried out at 20°C using the Protean IEF Cell (Bio-Rad, USA). After IEF, IPG strips were resolved in the second dimension using a 12.5% T, 2.6% C polyacrylamide gel buffered with 375 mM Tris buffer (pH 8.8), 0.1% (w/v) sodium dodecyl sulphate and polymerised with 0.05% (w/v) ammonium persulphate and 0.05% (v/v) tetramethylethylenediamine (TEMED). A stacking gel containing 5% T, 2.6% C polyacrylamide buffered with 375 mM Tris buffer (pH 6.8), 0.1% (w/v) SDS and 0.1% bromophenol blue was added to the resolving gel. The IPG strips were placed onto the stacking gel and overlaid with 0.5% (w/v) low melting agarose dissolved in 375 mM Tris (pH 8.8), with 0.1% (w/v) SDS. Electrophoresis was carried out at 4°C; 150V initially for 10 min then reduced to 90 V for 2.5 h.

Following electrophoresis, the gels were placed in fixative containing 10% methanol and 7% acetic acid for 1 h. The gels were then washed with distilled water for 20 min, 3 times and subsequently stained with colloidal coomassie blue (0.1% (w/v) CCB G-250,

2% (v/v) phosphoric acid, 10% (w/v) ammonium sulphate and 20% (v/v) methanol) for 20 h, with constant shaking at RT [11]; the gels were then de-stained 5 times with 0.5 M NaCl, 15 min each. Imaging of CCB-stained gels on the FLA-9000 imager (FUJIFILM, Tokyo, Japan) was carried out at 685/750 excitation/emission with a photomultiplier tube (PMT) setting of 600 V and pixel resolution set to 100  $\mu\text{m}$  [11]. Analysis of 2D gel images was performed using Delta 2D software with automated spot detection (Local Background Region: 96; Average Spot Size: 32 and sensitivity in percentage: 20.0) (version 4.0.8; DECODON GmbH, Gerifswald, Germany).

## 2.8. Mass Spectrometry

The following selection criteria were applied for spot inclusion. Changes in mean normalised spot volume (the abundance of resolved protein species) had to be greater than a 1.0 fold difference between samples from wild type versus V144D, C133W and C133Y mutants and be present in all replicate gels [11] [12]. Briefly, the protein species of interest were excised from gels and de-stained overnight. The gel pieces were then reduced and alkylated in 10 mM Dithiothreitol (DTT) and 15 mM Iodoacetic acid (IAA), and subsequently incubated with trypsin solution (10 ng/ $\mu\text{L}$ , pH 7.4) for 16 hours at 37°C. LC-MS/MS analysis was carried out on a nano Aquity UPLC (Waters Corp., Milford, MA, USA) linked to a XevoQToF mass spectrometer from Waters (Micromass, UK). The data were acquired using Masslynx software (Version 4.1, Micromass UK). The MS/MS data files were searched against Swiss Prot databases with semi-trypsin as the enzyme.

## 2.9. Calcium Imaging

ND15 cells were grown for 24 h in 35 mm glass bottom size 0 dish (MatTek, USA), and transfected as previously described. Molecular Probes Rhod-3 calcium imaging kit (Molecular Probes, USA) was used to stain the cells. Briefly, cells were incubated at RT in the dark for 1 h in 10  $\mu\text{M}$  Rhod-3 AM, 2.5 mM probenecid and 1 $\times$  power load. Cells were briefly washed in calcium-free PBS and incubated for a further 1 h at RT with 2.5 mM probenecid. To obtain low and high intracellular calcium images, NT ND15 cells were infused with PBS without calcium, containing 5 mM EGTA and 2  $\mu\text{M}$  ionomycin to allow intracellular calcium to efflux from the cell. High intracellular calcium images were obtained by infusing the cells in PBS containing calcium and 2  $\mu\text{M}$  ionomycin. Cells were ready for imaging after a further two washes in calcium-free PBS and imaged on the LSM 5 confocal microscope comprising the LSM 5 exciter laser scanning microscope with Axiovert 200M inverted optical microscope (Carl Zeiss, Jena, Germany).

## 3. Results

### 3.1. Expression of Proteins Identified in HSN-1 Transfected ND15 Cells

In order to assess the level of expression of proteins previously reported as altered, total cellular protein fractions from nontransfected, wild type and mutant HSN-I TT ND15 cells were isolated and quantitative immunoblot analyses were carried out (Figure 1).

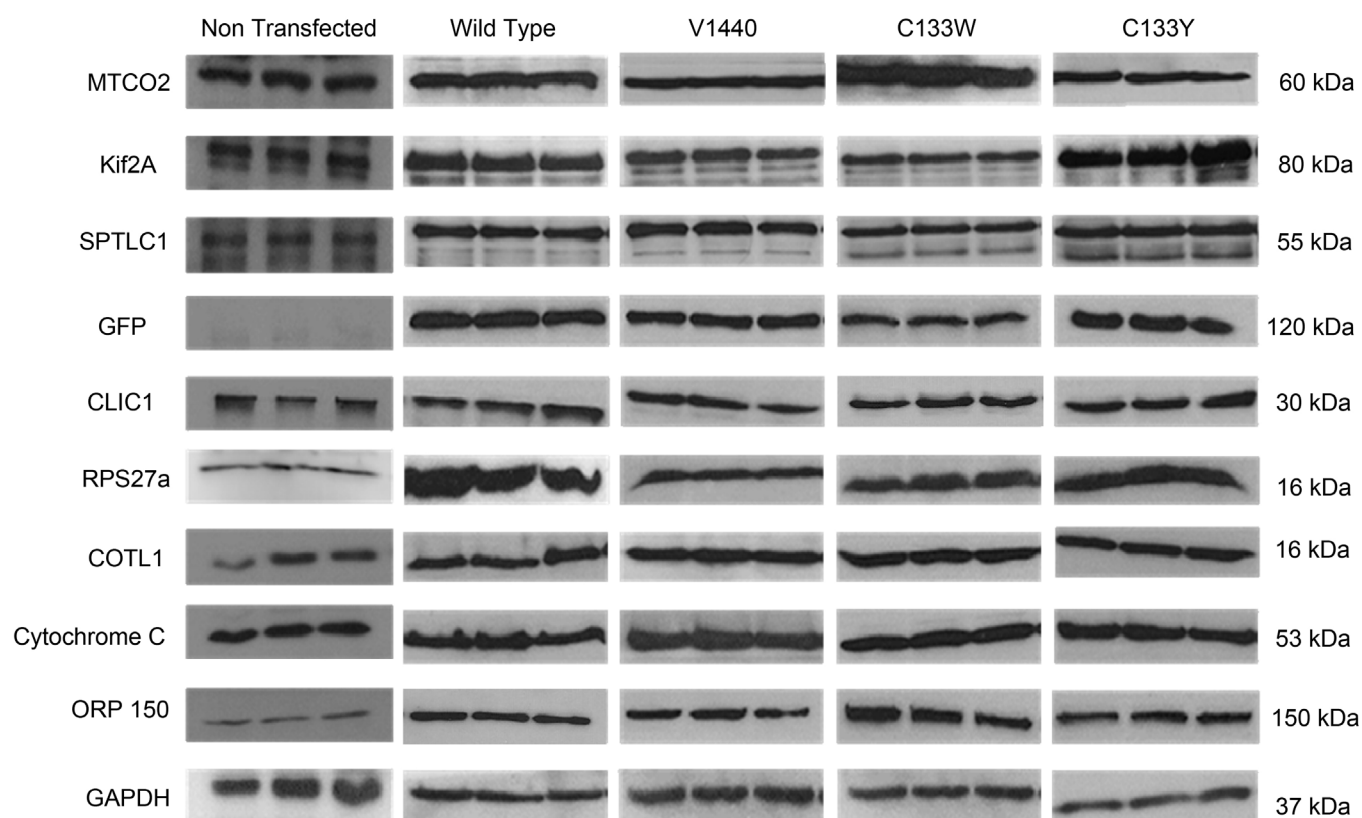
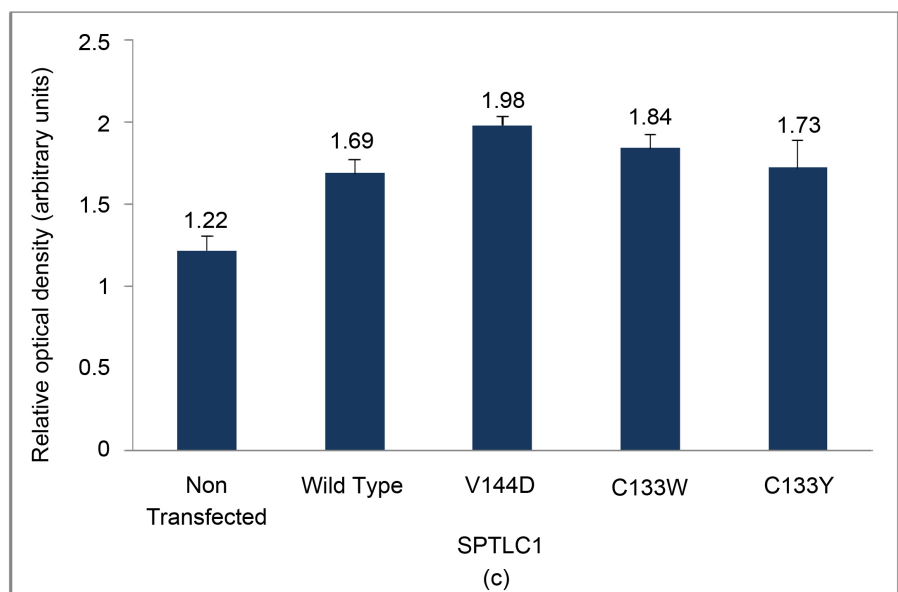
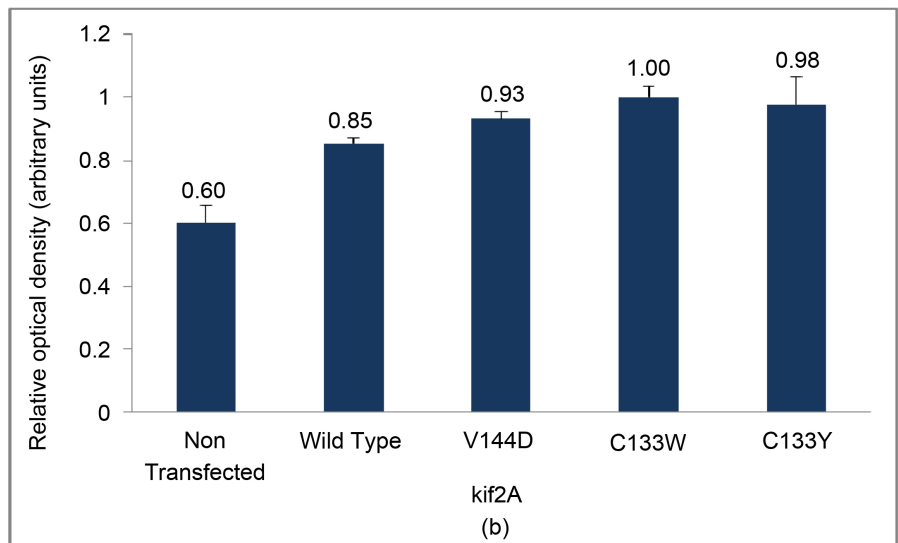
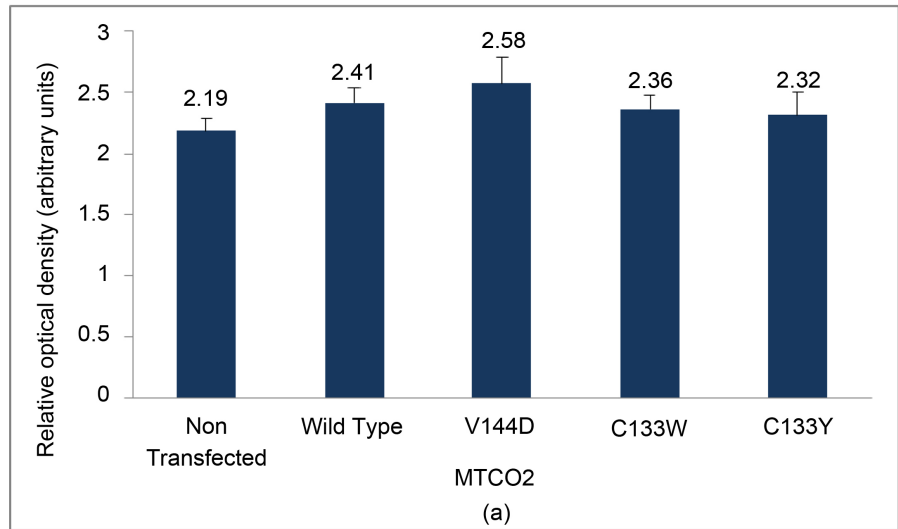


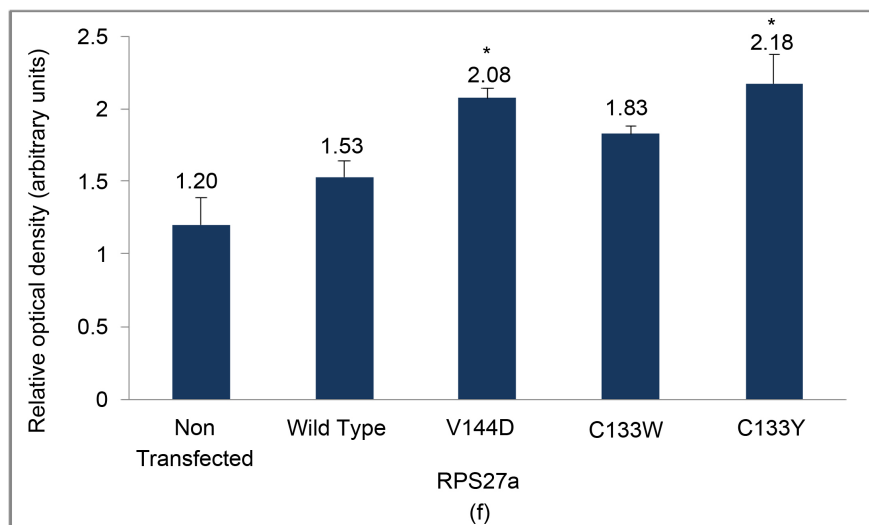
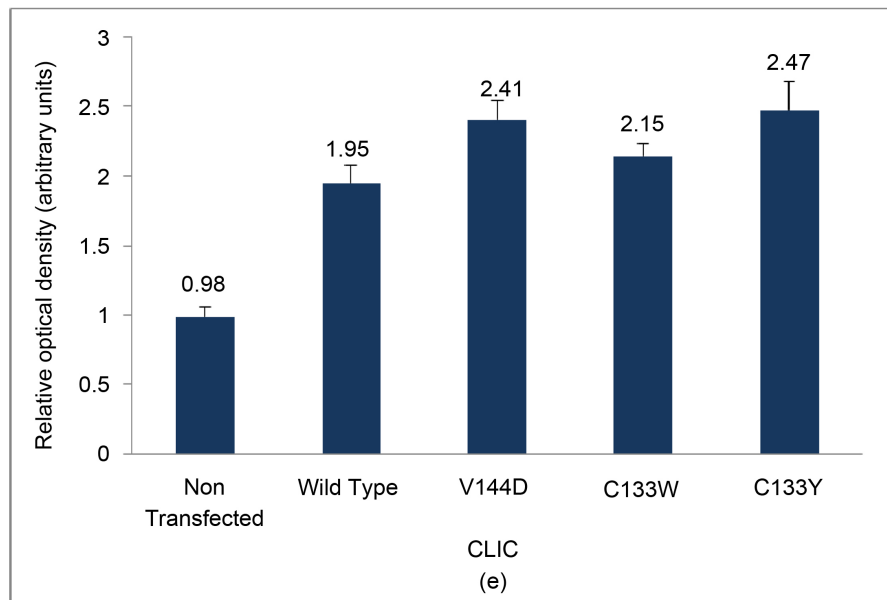
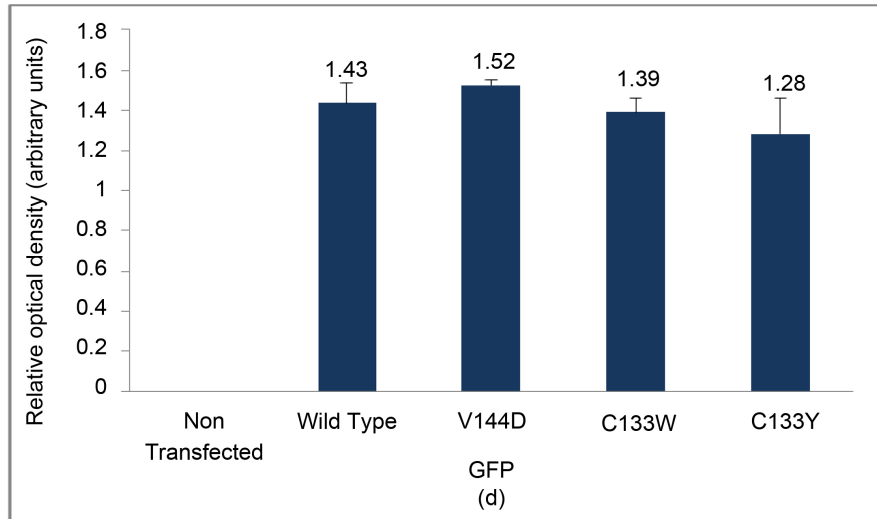
**Figure 1.** Immunoblots of proteins identified in nontransfected, wild type, V144D, C133W and C133Y transfected ND15 cells. 25  $\mu$ g of protein loaded per lane ( $n = 3$ ).

Quantitation of the immunoblot data (**Figures 2(a)-(j)**), confirmed that there were statistically significant ( $p < 0.05$ ) changes in expression of COTL1 (**Figure 2(g)**), Cytochrome C (**Figure 2(h)**) and ORP-150 (**Figure 2(i)**) in all mutants compared to the wild type, while RPS27a (**Figure 2(f)**) was significantly increased in V144D and C133Y. Although CLIC1 did not show any statistically significant increase in expression (**Figure 2(e)**), there was however an increase in expression in all mutants compared to the wild type. MTCO2 (**Figure 2(a)**), GFP (**Figure 2(d)**), SPTLC1 (**Figure 2(c)**), GAPDH (**Figure 2(j)**) and Kif2A (**Figure 2(b)**) showed no differential expression compared to the wild type.

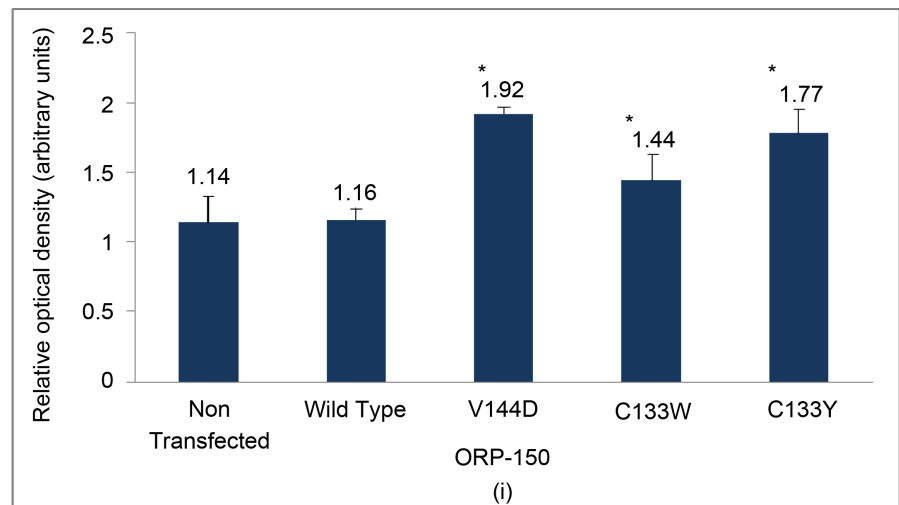
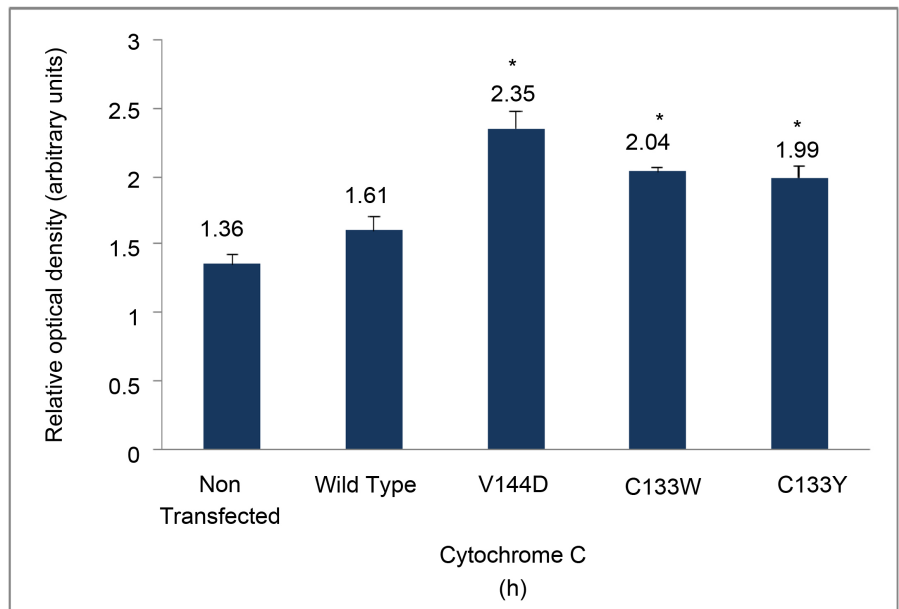
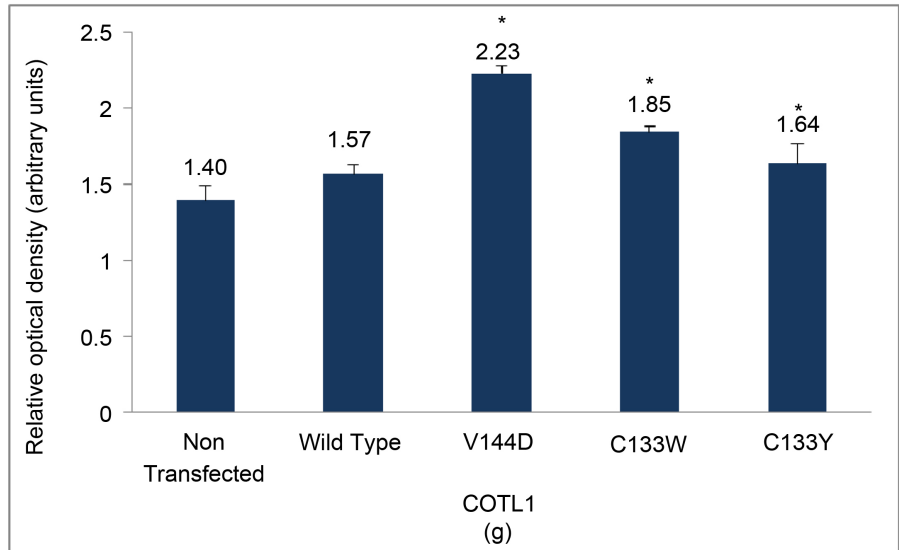
### 3.2. Intracellular Localisation Analyses of SPTLC1 and Proteins within Transiently Transfected ND15 Cells

The intracellular localisation and abundance of the proteins SPTLC1, Kif2A, Cytochrome C, RPS27a, CLIC1, ORP-150, COTL1 and MTCO2 were established using immunostained nontransfected, wild type and mutant TT ND15 cells. There were no apparent changes in intracellular localisation of the SPTLC1 when transfected with GFP labelled SPTLC1, which was found localised to the perinuclear region where the ER resides (**Figure 3(a)**). Kif2A is a microtubule associated protein distributed evenly across the cytoskeleton [14]. Kif2A displayed consistent cytoskeletal pattern throughout the









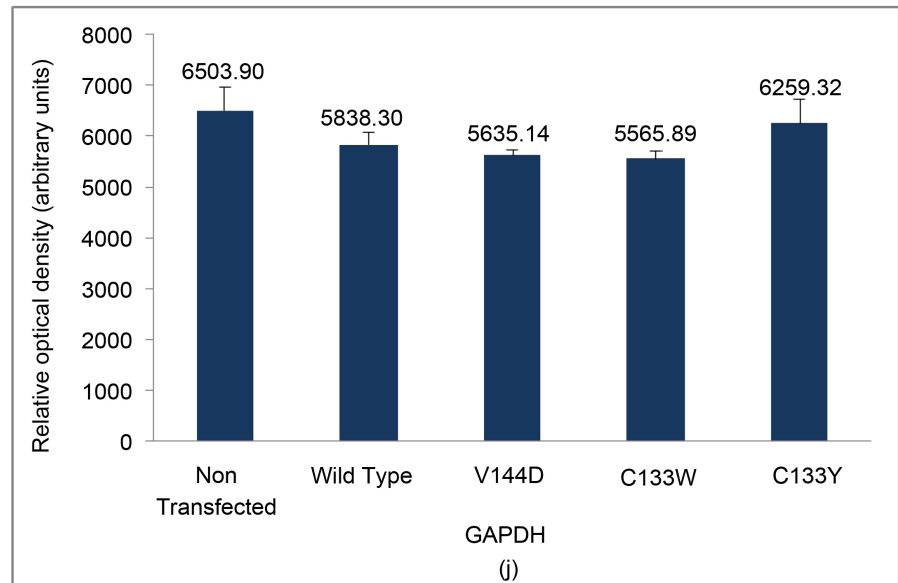


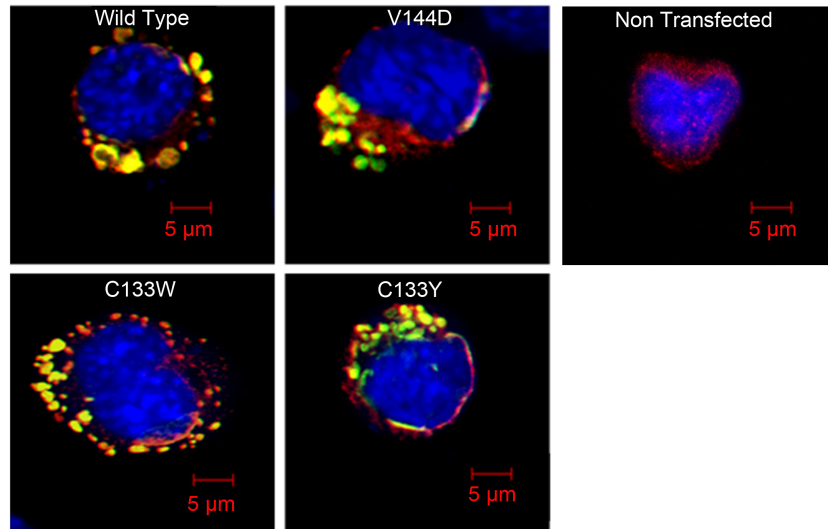
**Figure 2.** Expression of proteins in HSN-I transfected ND15 cells. Representative graphs showing the difference between nontransfected, wild type and mutant ND15 proteins. (a) MTCO2, (b) Kif2A, (c) SPTLC1, (d) GFP, (e) CLIC1, (f) RPS27a, (g) COTL1, (h) Cytochrome C, (i) ORP-150, and (j) GAPDH (\*)  $p < 0.05$  statistically significant increase ( $n = 3$ ). Errors bar depict SE of means. Blots were normalised to GAPDH.

cell in nontransfected, wild type and mutants (**Figure 3(b)**). MTCO2 is classically found to be distributed across the mitochondrial inner membrane. MTCO2 was distributed evenly throughout the mitochondria of the cells, indicating no change in the localisation within the mitochondria of mutant cells compared to the nontransfected and wild type cells (**Figure 3(h)**).

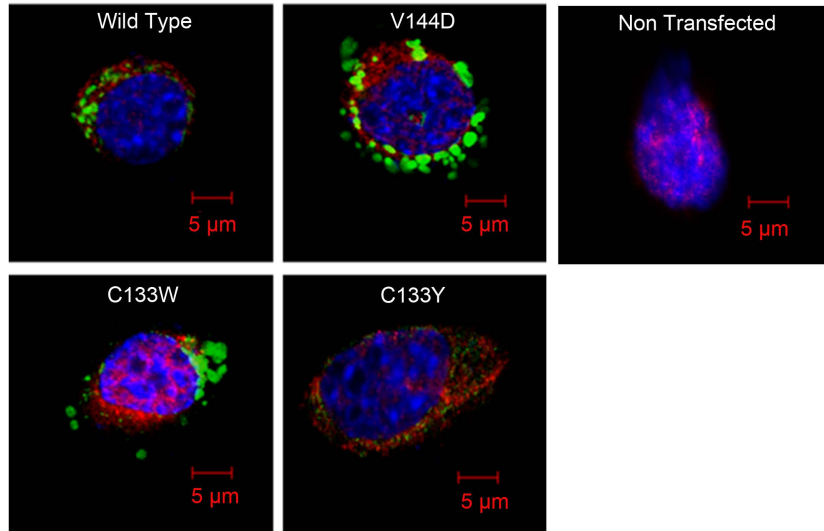
Cytochrome C is typically located within the mitochondrial inner membrane [15]. Interestingly, Cytochrome C showed a more perinuclear clustering in the mutant cells compared to that of the nontransfected and wild type cells, where the proteins were found to be more evenly distributed throughout the periphery of the cells (**Figure 3(c)**). RPS27a is located within the cytoplasm and nucleoplasm of cells [16]. With these proteins being evenly distributed throughout the cells in the nontransfected and wild type and mutants indicating no clustering of ubiquitinated proteins (**Figure 3(d)**). CLIC1 exists in a soluble and membrane bound form, typically distributed evenly within the cells [17]. CLIC1 was localised in the cell periphery in the nontransfected, wild type and mutant cells (**Figure 3(e)**). However the mutants displayed a larger localisation towards the perinuclear region, indicating that CLIC1 may be present more in the membrane form in the mutants.

ORP-150, a chaperon protein localised throughout the cell [18], was found to be distributed throughout the wild type and mutant cells. ORP-150 was also found to be more abundant within the mutants compared to the nontransfected and wild type cells (**Figure 3(f)**). COTL1 is a cytoskeletal associated protein interacting with the cytoskeleton [19]. COTL1 exhibited an even cytoskeletal pattern through all the cells. Interes-

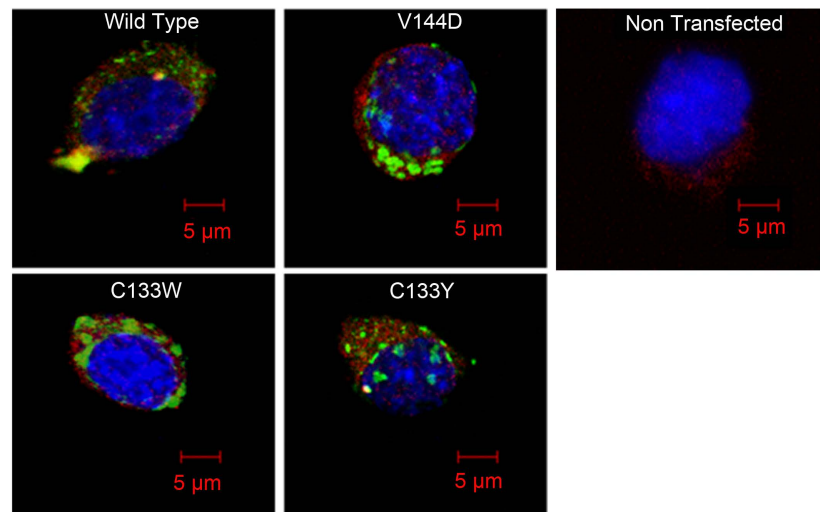
(a) SPTLC1



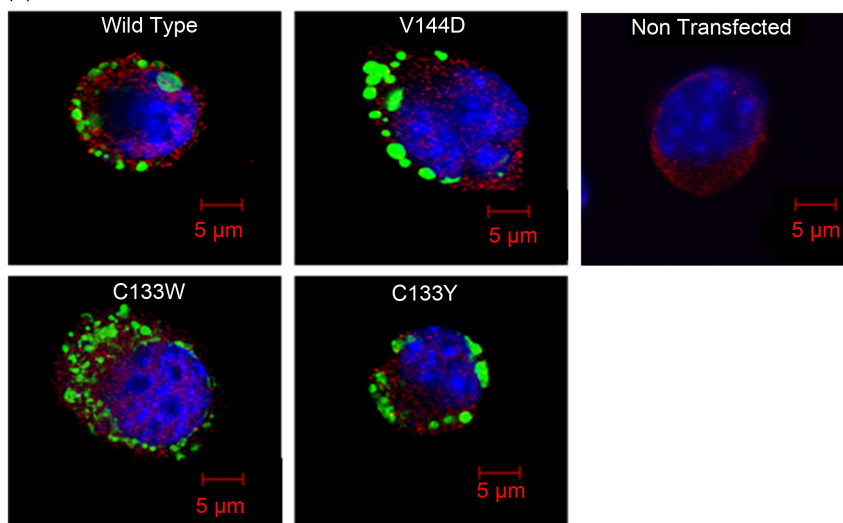
(b) Kif 2A



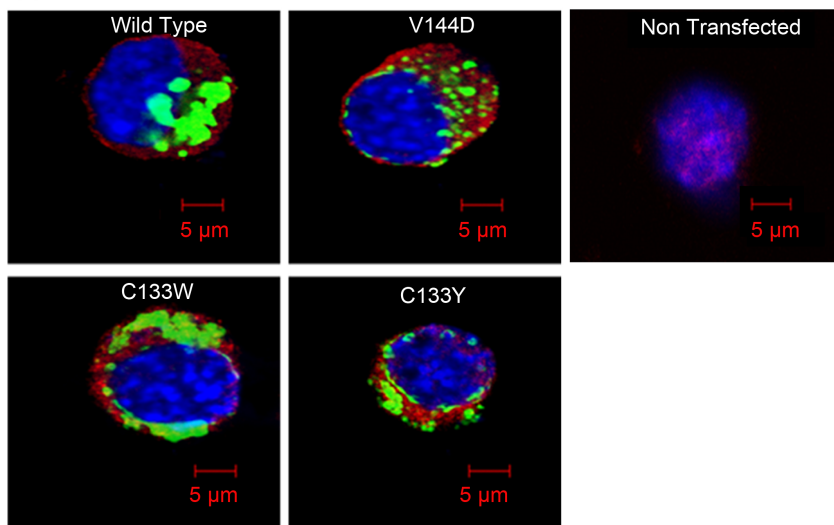
(c) Cytochrome C



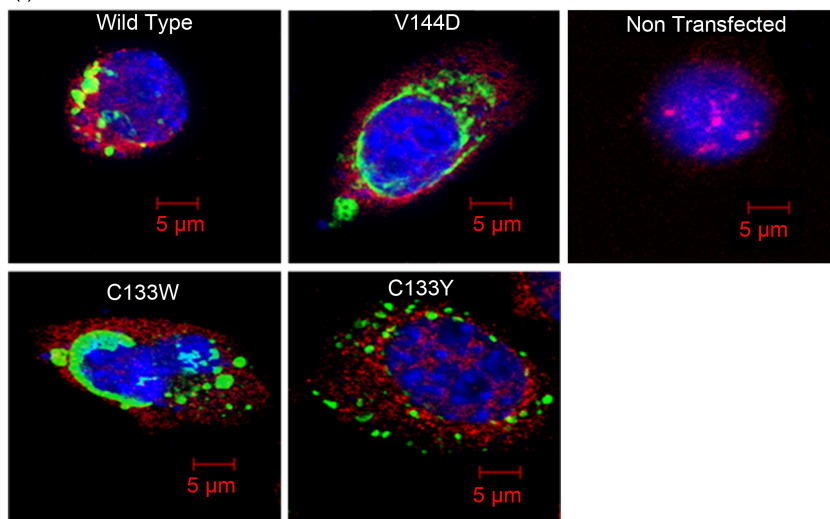
(d) RPS27a



(e) CLIC 1



(f) ORP 150



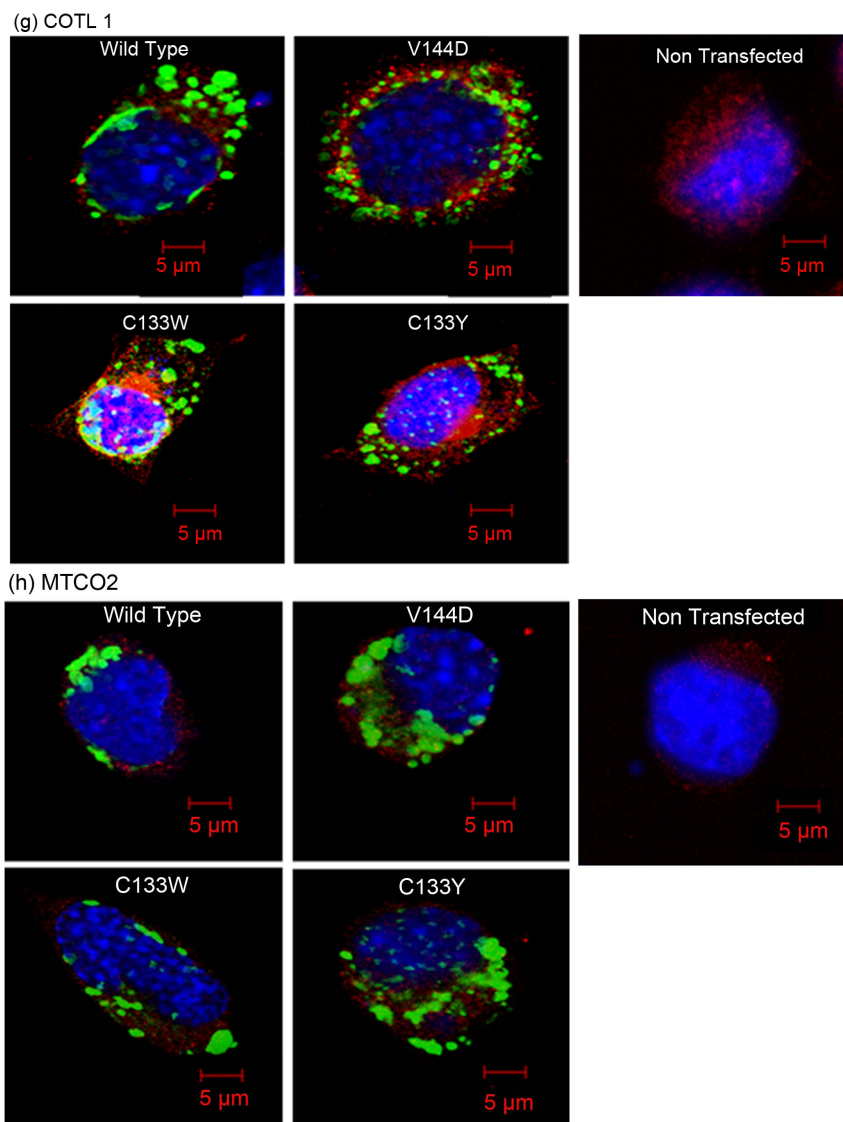


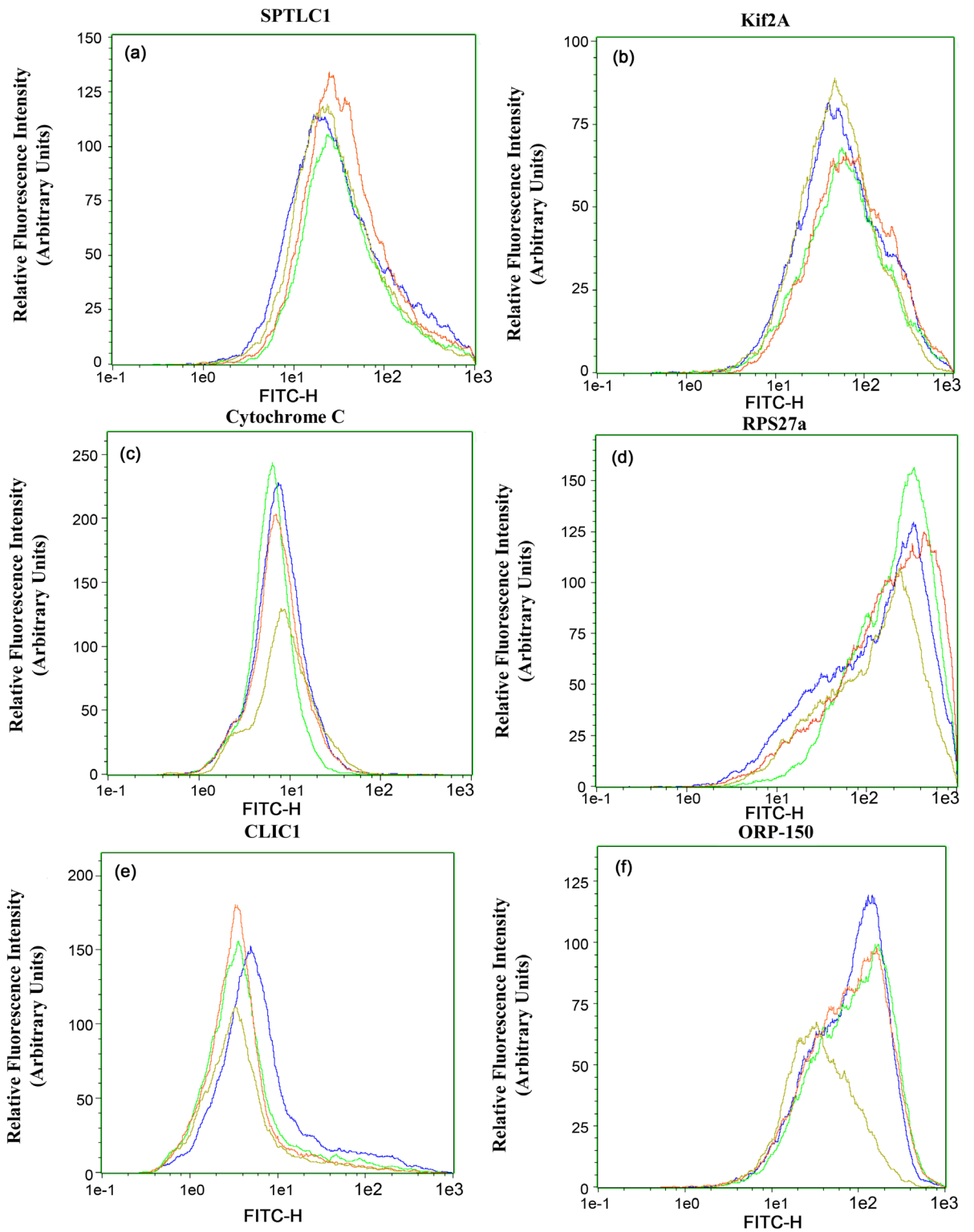
**Figure 3.** Representative immunofluorescence images of the intracellular localisation of proteins in transfected ND15 cells. Representative confocal micrographs showing (a) SPTLC1, (b) Kif2A, (c) Cytochrome C, (d) RPS27a, (e) CLIC1, (f) ORP-150, (g) COTL1 and (h) MTCO2 stained transfected (Green) ND15 cells (red) DAPI nuclear stain (blue). Scale bar = 5  $\mu$ m.

tingly, there appeared to be a more perinuclear clustering (as indicated by arrows, **Figure 3(g)**) and potential co-localisation in the C133W and C133Y mutants in comparison to the nontransfected and wild type cells.

### 3.3. FACS Analyses of Wild Type, V144D-, C133W- and C133Y-Transfected ND15 Cells Reveal Changes in Fluorescence Intensity of CLIC1, Cytochrome C, ORP-150 and RPS27a

Fluorescence assisted cell sorting (FACS) was used to determine the total fluorescence per cell of TT ND15 immunostained cells for the proteins SPTLC1, Kif2A, Cytochrome

C, RPS27a, CLIC1, ORP-150, COTL1, MTCO2 and GFP (Figure 4). There was a marked increase in the relative fluorescence intensity of CLIC1 (Figure 4(e)), Cytochrome C (Figure 4(c)), ORP-150 (Figure 4(f)) and RPS27a (Figure 4(d)) in the mutant



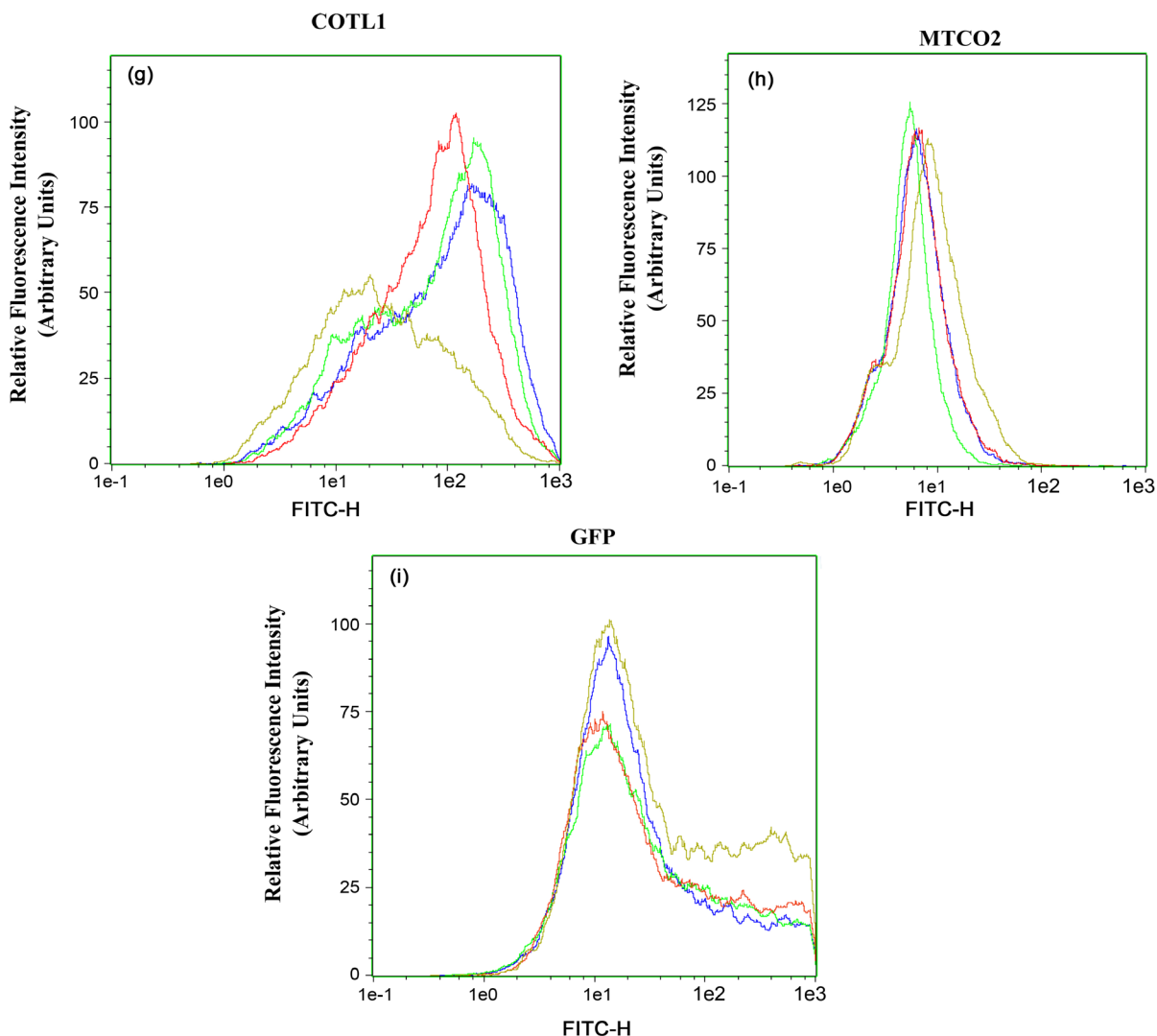


**Figure 4.** Relative quantification of Wild type, V144D, C133W and C133Y transfected ND15 cells. Flow cytometry analysis of the relative fluorescence intensity of (a) SPTLC1, (b) Kif2A (c) Cytochrome C (d) RPS27a (e) CLIC1 (f) ORP-150 (g) COTL1 (h) MTCO2 and (i) GFP. Gold histogram represents Wild Type, Blue histogram represents V144D, Green histogram represents C133W and Red histogram represents C133Y (n = 3).

cells compared to that of wild type. There were no changes to SPTLC1 (**Figure 4(a)**), Kif2A (**Figure 4(b)**) and GFP (**Figure 4(i)**) in the wild type and mutants. These results correlate with the quantitative immunoblot data presented in **Figure 2**.

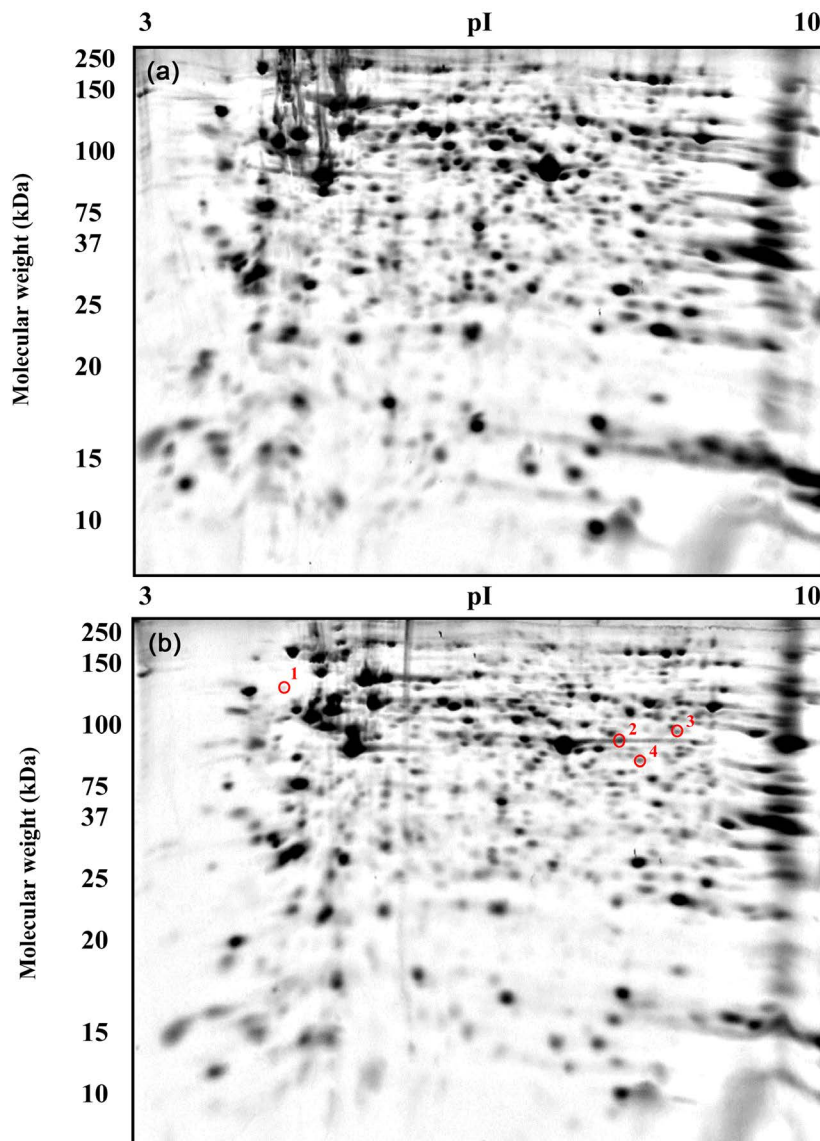
### 3.4. Resolution of Total Cellular Proteins Using 2D Gels from SPTLC1-Transfected ND15 Cells

Total isolated wild type and mutant ND15 proteins were resolved and quantitatively assessed using refined two dimensional gel electrophoresis (2DE) [10] [11]. The samples resolved covering the entire MW and pI range in triplicates (**Figure 5**). Standard spot counts indicated  $674 \pm 7$ ,  $669 \pm 4$ ,  $663 \pm 9$  and  $655 \pm 5$  protein species were resolved in wild type, V144D, C133W and C133Y mutant fractions respectively. LC/MS

data coupled with Mascot Daemon searches of SwissProt database resulted in identification of a further 14 protein alterations in the three mutant samples relative to the wild type, as summarised in **Table 1**.

### 3.5. Alterations within the Intracellular Calcium Levels of V144D-, C133W-, C133Y-Transfected ND15 Cells Compared to that of Wild Type and Nontransfected Controls

Wild type and mutant ND15 cells were analysed for total intracellular calcium using the Rhod-3 Am calcium stain (**Figure 6**). Cell images were analysed using ImageJ (NIH, USA) and corrected total cellular fluorescence was obtained. Analyses revealed a marked decrease in intracellular calcium in C133W and C133Y mutant cells. V144D mutant cells however, showed an increase in intracellular calcium when compared against basal levels determined in wild type and nontransfected (NT) cells (**Figure 7**).





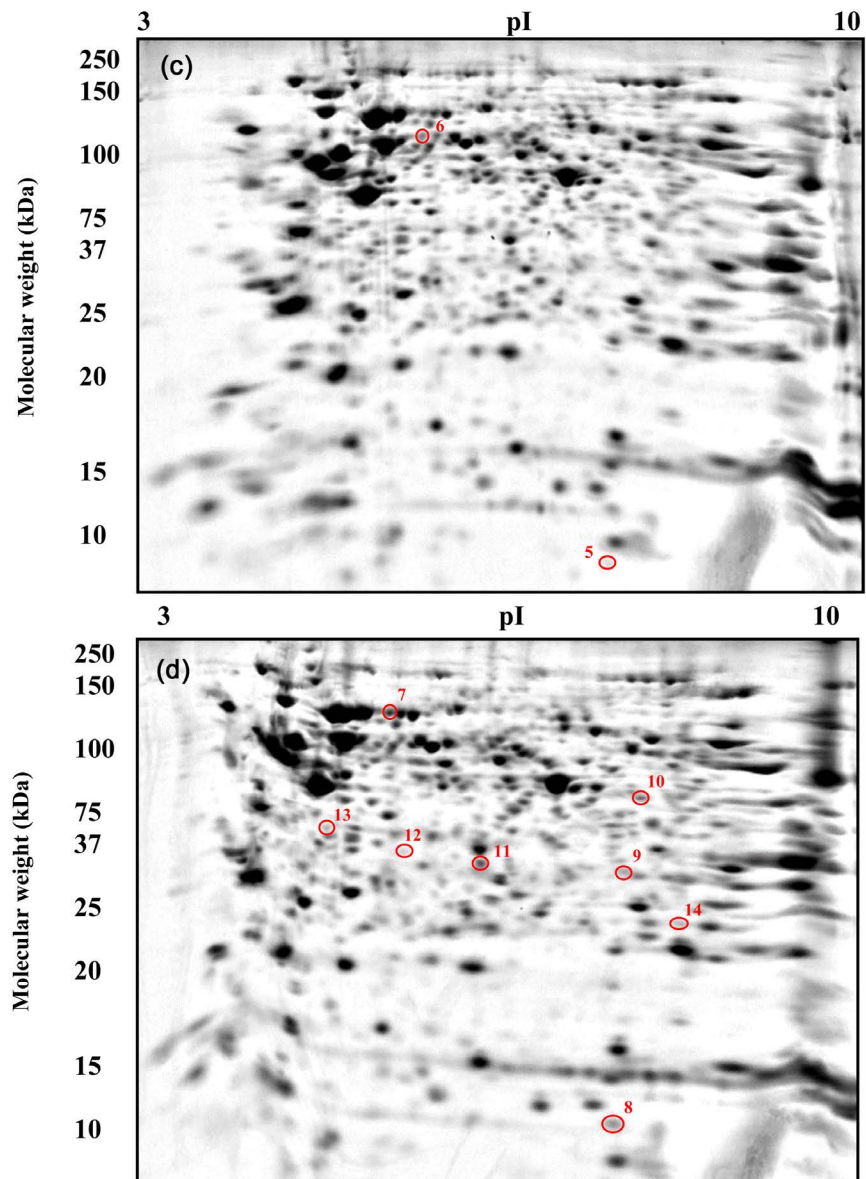


**Figure 5.** Representative images of 2D gels following resolution of total cellular proteins from HSN-1 transfected ND15 cells. (a) Wild type proteins (b) V144D proteins (c) C133W proteins and (d) C133Y proteins. The molecular weights are in kilo Daltons (kDa) and the IEF dimension is in pH units.

#### 4. Discussion

Mutations in the SPTLC1 subunit are known to be causal in HSN-I. Molecular and cellular studies of cells over-expressing the SPTLC1 mutations have identified potential dysfunction in sphingolipid biosynthesis and metabolic activity [4]. This investigation correlates the previous findings from the lymphoblast cell model done in our group [6] [7] [8] [13] with a neuronal cell model. In addition to the V144D mutation, we have also investigated changes within the C133W and C133Y mutations causing HSN-I.

Ubiquinol cytochrome C reductase core protein 1 is a central component of the

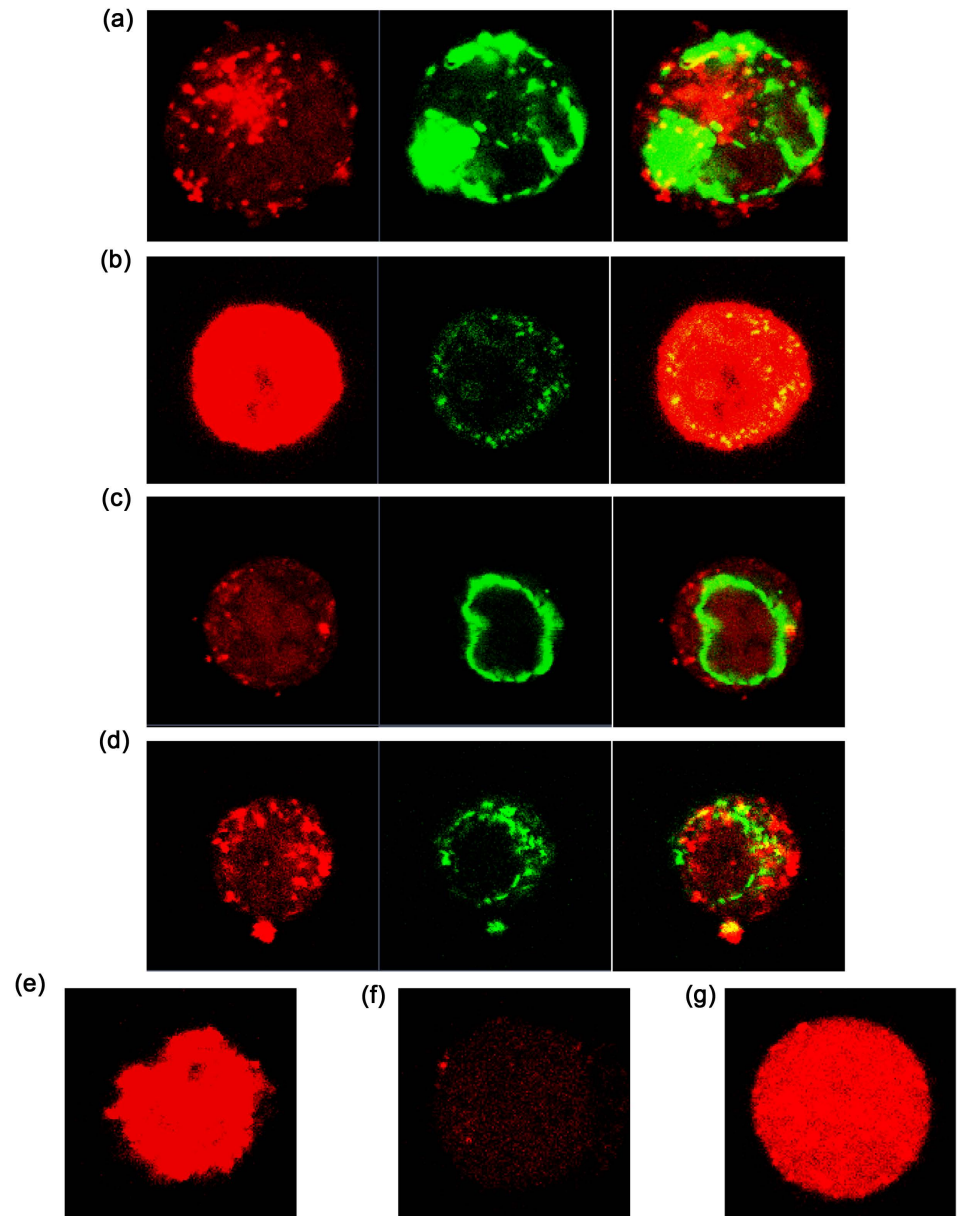


**Figure 6.** Representative confocal micrographs showing (a) Wild Type, (b) V144D, (c) C133W (d) C133Y (e) nontransfected (f) low Calcium (g) high intracellular calcium stained (red) ND15 cells showing GFP (Green). N = 25.

electron transport chain, catalysing the oxidation of ubiquinol and reduction of cytochrome C [15]. Here, we have shown in both quantitative protein expression (**Figure 2(h)**) and FACS analyses (**Figure 4(c)**) that cytochrome C expression was increased significantly in the TT ND15 cells containing the individual mutations. These findings thus strengthen the potential link to oxidative phosphorylation, *via* ubiquinol cytochrome C, and altered energy production ultimately leading to axonal degeneration.

Further quantitative analyses were carried out which confirmed that the protein expression of RPS27a (**Figure 2(f)**), COTL1 (**Figure 2(g)**), and ORP-150 (**Figure 2(i)**)

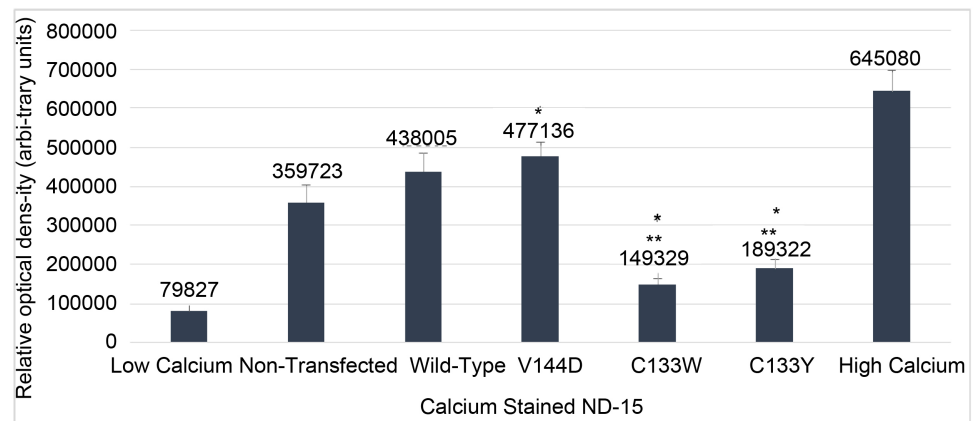


**Figure 7.** Relative intensity of intracellular calcium stained ND15 cells. Graph depicting relative optical density of calcium staining in NT, wild type and mutant ND15 cells ( $n = 25$ ). (\*)  $p < 0.05$ , vs nontransfected; (\*\*)  $p < 0.05$ , vs wild-type. Errors bar depict SE of means.

**Table 1.** Summary of mascot protein identification.

	Proteins Identified	Accession Number Matched	Unique Peptides	Sequence Coverage	Mascot Protein Score	Predicted pI	Predicted Mw (kDa)	Mascot pI	Mascot Mw (kDa)	Fold Increase or Decrease within the Mutant
1.	Protein Disulphide Isomerase	P09103	35	42%	1468	4.2	90	4.77	57.01	V144D-1.3 Fold ↓
2.	Alpha-Enolase	P17182	52	67%	1901	6.5	65	6.37	47.11	V144D-1.6 Fold ↑
3.	Long-chain specific acyl-CoA dehydrogenase	P51174	20	50%	1188	8.3	69	8.53	48.2	V144D-1.7 Fold ↑
4.	26s protease regulatory subunit 8	P62196	44	63%	1287	7.0	60	7.11	45.2	V144D-1.7 Fold ↑
5.	RPS27a	P62983	18	42%	193	9.2	16	8.00	9.68	C133W-2.6 Fold ↑
6.	Peptidyl-prolyl cis-trans isomerase	P30416	39	41%	576	5.4	90	5.54	57.6	C133W-1.7 Fold ↑
7.	Stress-70 protein, Mitochondrial	P38647	33	38%	884	4.3	75	5.81	73.70	C133Y-2.3 Fold ↑
8.	10 kDa heat shock protein, Mitochondrial	Q64433	3	37%	90	7.6	15	7.93	10.96	C133Y-3.5 Fold ↓
9.	Voltage-dependent anion-selective channel protein 2	Q60930	7	29%	229	7.9	30	7.44	32.34	C133Y-1.6 Fold ↑
10.	Long-chain specific acyl-CoA dehydrogenase, Mitochondrial	P51174	45	43%	1117	8.2	50	8.53	48.37	C133Y-2.1 Fold ↑
11.	26s Proteasome non-ATPase regulatory subunit 14	O35593	25	39%	580	5.8	30	6.06	34.77	C133Y-1.5 Fold ↑
12.	STIP1 homology and U box-containing protein 1	Q9WUD1	27	58%	366	5.9	35	5.71	35.34	C133Y-2.1 Fold ↓
13.	Eukaryotic Translation Initiator Factor 2 Subunit 1	Q6ZWX6	47	64%	944	4.5	37	5.02	36.37	C133Y-2.4 Fold ↓
14.	Triosephosphate Isomerase	P48500	34	79%	1162	8.5	26	6.89	27.4	C133Y-2.7 Fold ↓

were significantly increased in the V144D TT ND15 cells. These findings correlated with results previously identified in the lymphoblast model [6] [7]. In addition, COTL1

was significantly increased in the C133W and C133Y mutation. ORP-150 and RPS27a were found to be increased significantly in the C133Y mutation; however these proteins were increased in comparison to the wild type in C133W. FACS (**Figure 4**) analyses confirmed the altered expression of RPS27a (**Figure 4(d)**), CLIC1 (**Figure 4(e)**), ORP-150 (**Figure 4(f)**), and COTL1 (**Figure 4(g)**) in the TT mutant cells compared to that of the wild type.

The novel findings in this study indicate links to dysfunction in oxidative phosphorylation, *via* ubiquinol cytochrome C Reductase Core Protein 1 in all three mutations causing HSN-I. The increased expression of Cytochrome C results in the interference of energy production and oxidative stress upon the ER, eventually causing axonal retraction, a characteristic hallmark of HSN-I. Additionally, Stress-70 mitochondrial protein levels were identified in the C133Y mutant as being increased 2.3 fold relative to the wild type (**Figure 5**). When mitochondria are under stress, Stress-70 protein levels increase compensating for increased oxidative damage and maintain normal protein import and synthesis [20]. Thus, if mitochondrial oxidative stress is increased (potentially *via* ROS production), further cellular damage would occur, ultimately leading to impaired ER efficiency eventually resulting in ER stress.

It is evident that there is an increase in oxidative and ER stress within the cells containing HSN-I mutations. This is demonstrated by the increased expression of ORP-150, CLIC1, COTL1 and RPS27a. ORP-150 is an important molecular chaperone of the ER during stress [18]. CLIC1 is a redox-sensitive protein which usually exists in a soluble form in the cytoplasm but during times of stress undergoes structural changes and inserts into lipid membranes [17]. COTL1 is an actin binding partner with upregulation in response to stress upon the cytoskeletal system [19]. Taken together, these data strongly suggests that oxidative stress could be linked to increases in ubiquinol cytochrome C. Thus, an increase in ORP-150 potentially compensates and protects the cell from an increase in ROS production, causing a shift in CLIC1 expression and stabilisation of the cytoskeleton *via* COTL1. RPS27a is responsible for targeting misfolded proteins for destruction, with an apparent increase highlighting potential increases in misfolded proteins and protein aggregation due to oxidative stress [16].

Further strengthening the connection between ER stress and HSN-I, peptidyl-prolyl cis-trans isomerase was found to be increased in abundance by 1.7 fold in the C133W mutant. This protein ensures newly synthesised proteins are folded into their correct conformation [21]. The 26 s proteasome is responsible for regulating the proteome through degradation of ubiquitin-tagged substrates [22]. 26 s proteasome regulatory subunit 8 was found to be increased in abundance by 1.7 fold in the V144D mutation [22]. The increase in abundance of these two proteins coupled with the increased expression of RPS27a and ORP-150 highlights the possible increased oxidative stress affecting protein folding conformation.

## 5. Conclusions

Calcium is an important signaling molecule involved in the regulation of many cellular

functions. Mitochondrial calcium uptake has been shown to lead to free radical production, with a delicate balance existing between moderate ROS production to modulate physiological signaling and overproduction of ROS which can ultimately lead to oxidative and ER stress [23] [24]. Decreases in calcium are believed to be a cellular response to increased stress, serving as a mechanism to limit further damage and increase cell survival [24]. As part of this study, we examine the intracellular levels of calcium in wild type, V144D, C133W, and C133Y. Whilst intracellular calcium is decreased within C133W and C133Y, calcium within the V144D mutation is increased. Hence, is the increased level of calcium a correlation of ER stress and mitochondrial dysfunction occurring, and the result of the V144D-mutation being unable to reduce intracellular calcium to compensate and protect the cell? Could this difference give insight into how the three mutations differ, ultimately causing HSN-I? Further investigation into intracellular and mitochondrial calcium levels is required to delineate the differences within the three mutations.

This investigation has shown a correlation between previous studies, revealing an increase in a mitochondrial electron transport chain protein, increases in proteins induced by oxidative stress and changes in the intracellular calcium levels in all three SPTLC1 mutations causing HSN-I. These findings provide further evidence for mitochondrial and ER dysfunction occurring as a result of mutations in SPTLC1. These novel findings provide critical new directions in understanding the underlying molecular and cellular alterations broadly applicable (and specific) to all mutations causing HSN-I and neurodegenerations as a whole.

## References

- [1] Dawkins, J.L., Hulme, D.J., Brahmabhatt, S.B., Auer-Grumbach, M. and Nicholson, G.A. (2001) Mutations in SPTLC1, Encoding Serine Palmitoyltransferase, Long Chain Base Subunit-1, Cause Hereditary Sensory Neuropathy Type I. *Nature Genetics*, **27**, 309-312. <https://doi.org/10.1038/85879>
- [2] Hanada, K. (2003) Serine Palmitoyltransferase: A Key Enzyme of Sphingolipid Metabolism. *Biochimica et Biophysica Acta*, **1632**, 16-30. [https://doi.org/10.1016/S1388-1981\(03\)00059-3](https://doi.org/10.1016/S1388-1981(03)00059-3)
- [3] Verhoeven, K., Coen, K., De Vriendt, E., Jacobs, A., Van Gerwen, V., Smouts, I., Pou-Ser-radell, A., Martin, J.J., Timmerman, V. and De Jonghe, P. (2004) SPTLC1 Mutation in Twin Sisters with Hereditary Sensory Neuropathy Type I. *Neurology*, **62**, 1001-1002. <https://doi.org/10.1212/01.WNL.0000115388.10828.5C>
- [4] Wei, J., Yerokun, Y., Liepelt, M., Momin, A., Wang, E., Hanada, K. and Merrill Jr., A.H. (2007) 2-1 Serine Palmitoyltransferase. In: Hirabayashi, Y., Igarashi, Y. and Merrill Jr., A.H., Eds., *Sphingolipid Biology*, Springer, Berlin, 25-27.
- [5] Dyck, P.J. and Thomas, P.K. (2005) *Dyck: Peripheral Neuropathy*. 4th Edition, Mosby, Philadelphia.
- [6] Stimpson, S.E., Coorssen, J.R. and Myers, S.J. (2015) Mitochondrial Protein Alterations in a Familial Peripheral Neuropathy Caused by Mutations in the Sphingolipid Protein, SPTLC1. *Journal of Biological Chemistry*, **8**, 25-35. <https://doi.org/10.1007/s12154-014-0125-x>
- [7] Stimpson, S.E., Coorssen, J.R. and Myers, S.J. (2016) Isolation and Identification of ER As-

- sociated Proteins with Unique Expression Changes Specific to the V144D SPTLC1 Mutations in HSN-I. *Analytical Biochemistry*, **5**, 248.
- [8] Stimpson, S.E., Coorsen, J.R. and Myers, S.J. (2015) Proteome Alterations Associated with the V144D SPTLC1 Mutation That Causes Hereditary Sensory Neuropathy-I. *Electronic Journal of Biology*, **11**, 176-186.
- [9] Churchward, M., Butt, R.H., Lang, J., Hsu, K. and Coorsen, J. (2005) Enhanced Detergent Extraction for Analysis of Membrane Proteomes by Two-Dimensional Gel Electrophoresis. *Proteome Science*, **3**, 5. <https://doi.org/10.1186/1477-5956-3-5>
- [10] Butt, R.H. and Coorsen, J.R. (2005) Postfractionation for Enhanced Proteomic Analyses: Routine Electrophoretic Methods Increase the Resolution of Standard 2D-PAGE. *Journal of Proteome Research*, **4**, 982-991. <https://doi.org/10.1021/pr050054d>
- [11] Gauci, V.J., Padula, M.P. and Coorsen, J.R. (2013) Coomassie Blue Staining for High Sensitivity Gel-Based Proteomics. *Journal of Proteomics*, **90**, 96-106. <https://doi.org/10.1016/j.jprot.2013.01.027>
- [12] Wright, E.P., Partridge, M.A., Padula, M.P., Gauci, V.J., Malladi, C.S. and Coorsen, J.R. (2014) Top-Down Proteomics: Enhancing 2D Gel Electrophoresis from Tissue Processing to High-Sensitivity Protein Detection. *Proteomics*, **14**, 872-889. <https://doi.org/10.1002/pmic.201300424>
- [13] Myers, S., Malladi, C., Hyland, R., Bautista, T., Boadle, R., Robinson, P. and Nicholson, G. (2014) Mutations in the SPTLC1 Protein Cause Mitochondrial Structural Abnormalities and Endoplasmic Reticulum Stress in Lymphoblasts. *DNA and Cell Biology*, **33**, 399-407. <https://doi.org/10.1089/dna.2013.2182>
- [14] Jang, C.Y., Wong, J., Coppinger, J.A., Seki, A., Yates, J.R. and Fang, G. (2008) DDA3 Recruits Microtubule Depolymerase Kif2a to Spindle Poles and Controls Spindle Dynamics and Mitotic Chromosome Movement. *Journal of Cell Biology*, **181**, 255-267. <https://doi.org/10.1083/jcb.200711032>
- [15] Crofts, A.R. (2004) The Cytochrome bc<sub>1</sub> Complex: Function in the Context of Structure. *Annual Review of Physiology*, **66**, 689-733. <https://doi.org/10.1146/annurev.physiol.66.032102.150251>
- [16] Hallengren, J., Chen, P.C. and Wilson, S.M. (2013) Neuronal Ubiquitin Homeostasis. *Cell Biochemistry and Biophysics*, **67**, 67-73. <https://doi.org/10.1007/s12013-013-9634-4>
- [17] Veraimo, S., Milton, R.H., Duchon, M.R. and Mazzanti, M. (2010) Chloride Intracellular Channel 1 (CLIC1): Sensor and Effector during Oxidative Stress. *FEBS Letters*, **584**, 2076-2084. <https://doi.org/10.1016/j.febslet.2010.02.073>
- [18] Behnke, J. and Hendershot, L.M. (2014) The Large Hsp70 Grp170 Binds to Unfolded Protein Substrates *in Vivo* with a Regulation Distinct from Conventional Hsp70s. *Journal of Biological Chemistry*, **289**, 2899-2907. <https://doi.org/10.1074/jbc.M113.507491>
- [19] Provost, P., Doucet, J., Stock, A., Gerisch, G., Samuelsson, B. and Radmark, O. (2001) Coactosin-Like Protein: A Human F-Actin-Binding Protein: Critical Role of Lysine-75. *Biochemical Journal*, **359**, 255-263. <https://doi.org/10.1042/bj3590255>
- [20] Herrmann, J.M., Stuart, R.A., Craig, E.A. and Neupert, W. (1994) Mitochondrial Heat Shock Protein 70, a Molecular Chaperone for Proteins Encoded by Mitochondrial DNA. *Journal of Cell Biology*, **127**, 893-902. <https://doi.org/10.1083/jcb.127.4.893>
- [21] Shaw, P.E. (2002) Peptidyl-Prolyl Isomerases: A New Twist to Transcription. *EMBO Reports*, **3**, 521-526. <https://doi.org/10.1093/embo-reports/kvf118>
- [22] Matyskiela, M.E., Lander, G.C. and Martin, A. (2013) Conformational Switching of the 26S Proteasome Enables Substrate Degradation. *Nature Structural & Molecular Biology*, **20**,

781-788. <https://doi.org/10.1038/nsmb.2616>

- [23] Glancy, B. and Balaban, R.S. (2012) Role of Mitochondrial Ca<sup>2+</sup> in the Regulation of Cellular Energetics. *Biochemistry*, **51**, 2959-2973. <https://doi.org/10.1021/bi2018909>
- [24] Feissner, R.F., Skalska, J., Gaum, W.E. and Sheu, S.S. (2009) Crosstalk Signaling between Mitochondrial Ca<sup>2+</sup> and Ros. *Frontiers in Bioscience*, **14**, 1197-1218. <https://doi.org/10.2741/3303>



Scientific Research Publishing

**Submit or recommend next manuscript to SCIRP and we will provide best service for you:**

Accepting pre-submission inquiries through Email, Facebook, LinkedIn, Twitter, etc.

A wide selection of journals (inclusive of 9 subjects, more than 200 journals)

Providing 24-hour high-quality service

User-friendly online submission system

Fair and swift peer-review system

Efficient typesetting and proofreading procedure

Display of the result of downloads and visits, as well as the number of cited articles

Maximum dissemination of your research work

Submit your manuscript at: <http://papersubmission.scirp.org/>

Or contact [wjns@scirp.org](mailto:wjns@scirp.org)